Plant, Cell & Environment

Plant, Cell and Environment (2012) **35**, 1109–1120 doi: 10.1111/j.1365-3040.2011.02476.x

Plasmodesmatal pores in the torus of bordered pit membranes affect cavitation resistance of conifer xylem

S. JANSEN[1]*, J.-B. LAMY[2], R. BURLETT[2], H. COCHARD[3], P. GASSON[1] & S. DELZON[2]

[1]Jodrell Laboratory, Royal Botanic Gardens, Kew, Richmond, Surrey TW9 3DS, UK, [2]INRA, University of Bordeaux, UMR BIOGECO, Talence, France and [3]INRA, UMR 547 PIAF, F-63100 Clermont-Ferrand, France

ABSTRACT

The pit membrane in bordered pits of conifer tracheids is characterized by a porous margo and central thickening (torus), which is traditionally considered to function as an impermeable safety valve against air-seeding. However, electron microscopy based on 33 conifer species, including five families and 19 genera, reveals that pores occur in the torus of 13 of the species studied. The pores have a plasmodesmatal origin with an average diameter of 51 nm and grouped arrangement. Evidence for embolism spreading via pores in tori is supported by the pore sizes, which correspond relatively well with the pressure inducing cavitation. Predictions based on earlier correlations between pit structure and cavitation resistance were only weakly supported for species with punctured tori. Moreover, species with punctured tori are significantly less resistant to cavitation than species with non-punctured tori. Nevertheless, absolute pore diameters must be treated with caution and correlations between theoretical and measured air-seeding pressures are weak. Because most pores appear not to traverse the torus but are limited to one torus pad, only complete pores would trigger air-seeding. Embolism spreading through a leaky torus is not universal across gymnosperms and unlikely to represent the only air-seeding mechanism.

Key-words: air-seeding; conifer wood; torus-margo; tracheid.

INTRODUCTION

The study of bordered pits and their biological significance in xylem has fascinated plant anatomists for centuries (Choat, Cobb & Jansen 2008). Soon after understanding that a pit membrane represents the primary wall that runs between the bordered pit cavities of a pit pair (Schacht 1859), much attention has been paid to conifer pit membranes with a 'torus', which represents the central thickening of the pit membrane and is surrounded by a porous 'margo' (Von Nägeli 1864; Sanio 1873; Russow 1883; Strasburger 1891; Liese 1965; Bauch, Schultze & Liese 1972). Pit membranes are of special interest for understanding structure – function relationships of water transport because they determine hydraulic efficiency for water flow between neighbouring tracheary elements, and limit the passage of air bubbles and pathogens into the sap stream (Tyree & Zimmermann 2002; Choat *et al.* 2008; Jansen, Choat & Pletsers 2009). Interest in the function of pit membranes is also due to their role in the movement of liquids and gas within wood and their influence on the permeability, drying and pulping of timber (Flynn 1995; Singh *et al.* 1999; Bao, Lu & Zhao 2001; Usta & Hale 2006).

As the porosity of tracheid walls is highest where there are pits, drought-induced cavitation is thought to occur at the pit level by a process called 'air-seeding' (Sperry & Tyree 1988, 1990; Tyree & Zimmermann 2002). The functional explanation for the nature of torus-margo pit membranes in conifers is that tori behave as safety valves, which are able to block off the pit aperture where there is a pressure difference between adjacent tracheids (Bailey 1913, 1916; Hart & Thomas 1967; Cochard *et al.* 2009). When a torus is in its relaxed, unaspirated position, the thin and porous margo is shown to offer a pit-area resistance that is on average 59 times lower than an angiosperm pit membrane (Hacke, Sperry & Pittermann 2004; Pittermann *et al.* 2005, 2010; Pittermann 2010). Aspirated tori, however, prevent the spreading of air into neighbouring tracheids. This sealing mechanism seems to be valid up to a certain threshold and air-seeding will occur when the pressure drop difference between adjacent tracheids exceeds a certain limit (Cochard *et al.* 2009; Delzon *et al.* 2010). The exact location of the air-seeding mechanism, however, remains unclear and two likely hypotheses have been proposed: (1) seal capillary-seeding (i.e. the torus does not perfectly seal the outer pit aperture, allowing air bubbles to pass through micropores at the edge of the torus); and (2) torus capillary-seeding (i.e. air-seeding through pores in the torus) (Delzon *et al.* 2010). Recent studies also demonstrate that anatomical features correlated with air-seeding in conifer tracheids mainly include torus thickness and the ratio of the torus to pit aperture diameter, but do not vary systematically with

---

Correspondence: S. Jansen. Fax: +49 731 502 3320; e-mail: steven.jansen@uni-ulm.de

*Present address: Institute of Systematic Botany and Ecology, Albert-Einstein-Allee 11, Ulm University, D-89081 Ulm, Germany. Contributors: S.J. and J.-B.L. contributed equally to this study and are both considered as first authors.

margo porosity (Cochard *et al*. 2009; Hacke & Jansen 2009; Delzon *et al*. 2010; Pittermann *et al*. 2010).

The traditional understanding of air-seeding in bordered pits of conifers is based on the assumption that tori are impermeable to water and air, and that the valve mechanism depends on the elastic properties of the margo (Liese & Johann 1954; Liese 1965; Liese & Bauch 1967; Comstock & Côté 1968; Bao *et al*. 2001; Hacke *et al*. 2004). Therefore, the thick and non-porous nature of the torus plays a crucial role in the safety valve hypothesis. However, earlier observations suggested the presence of minute pores in the torus of *Abies firma*, *Abies sachalinensis*, *Pinus koraiensis*, *Pinus palustris*, *Pinus serotina*, *Pinus taeda*, *Pinus wallichiana* and *Tsuga sieboldii* (Thomas 1969; Thomas & Nicholas 1969; Fujikawa & Ishida 1972; Panshin & De Zeeuw 1980; Sano, Kawakami & Ohtani 1999; Dute, Hagler & Black 2008; Roth-Nebelsick, Voigt & Gorb 2010). Thomas (1969) suggested that the openings in tori of *Pinus* represent plasmodesmata because of their circular depression and raised central position. More recent observations in *A. firma* showed that the pores in tori of mature pit membranes correspond to channels of secondary (i.e. post-cytokinetically formed) plasmodesmata (Dute *et al*. 2008). Furthermore, Sano *et al*. (1999) demonstrated that the frequency of tori with pores varied from 45 to 81% across the innermost and middle area of the last three growth rings in *A. sachalinensis*. While some earlier observations of micropores in the torus of conifer pit membranes were interpreted as preparation artefact (Jansen, Pletsers & Sano 2008), cryo-scanning electron microscopy (SEM) demonstrated that pores detected in *P. wallichiana* represent real features associated with the native state of pit membranes (Roth-Nebelsick *et al*. 2010).

Taxonomic implications and functional consequences for conifers with punctured tori remain unclear. Minute openings in tori have recently been suggested as a functional explanation for the air-seeding mechanism in gymnosperms (Cochard *et al*. 2009; Delzon *et al*. 2010). Therefore, we hypothesize that the occurrence and the size of pores associated with tori are correlated with vulnerability to xylem cavitation, which is known to vary extensively within conifers (Maherali, Pockman & Jackson 2004; Delzon *et al*. 2010; Pittermann *et al*. 2010). The two major aims of this study are: (1) to explore the distribution of tori with pores across gymnosperms; and (2) to test whether these pores could represent sites of air-seeding associated with drought-induced cavitation. Both goals will be addressed by sampling across a broad taxonomic range of gymnosperms and by exploring in detail what aspects of pit structure are related to the variation in cavitation resistance. In particular, earlier hypotheses regarding cavitation resistance and pit morphology will be evaluated for the species with punctured tori. Overall, this paper aims to better understand the structural basis of cavitation resistance, which is a major issue in identifying the genetic background of drought resistance in plants.

MATERIALS AND METHODS

Plant material

A total of 33 conifer species was investigated, covering 5 families and 19 genera (Table 1). As we aimed to examine three to five specimens per species, criteria for species selection were: (1) the availability of three to five mature and healthy trees for each species; and (2) the taxonomic position, aiming to include species with a taxonomic range as broad as possible. For *Pinus nigra* and *P. wallichiana*, only one specimen was collected. Most trees sampled were growing at the Royal Botanic Gardens, Kew (UK) with an average daily temperature of 10.8 °C and 605 mm of annual rainfall.

Straight branches fully exposed to the sun were collected from each tree where they were most conveniently reached. The samples were longer than 40 cm and the xylem was 3–10 mm in diameter. Compression wood was avoided, and needles were removed as soon as possible in order to stop transpiration. The fresh stem segments were then immediately wrapped in wet paper towels and plastic bags, and brought to the laboratory.

Scanning electron microscopy

SEM observations were conducted on air-dried samples that were used for measuring cavitation resistance. Although intraspecific variation of pit morphology can be significant (Domec *et al*. 2008; Jansen *et al*. 2009; Schoonmaker *et al*. 2010; Gortan *et al*. 2011), qualitative features such as the presence or absence of punctured tori were assumed to be consistently present or absent for a given species. Although this assumption was only tested on observations for two species (*Pinus hartwegii* and *Pinus pinaster*), our approach mainly aimed at studying the taxonomic variation of pores in tori across various conifer genera and families. Therefore, SEM observations were limited to one sample for most species. We selected the sample that was closest to the average P_{50} value for each species.

SEM preparation followed standard protocols, except that the samples were briefly treated in an alcohol series (50, 70, 90, 100% ethanol) for a total of 5 min in order to remove pit membrane encrustations that could make detection of pores difficult (Thomas 1969; Jansen *et al*. 2008, 2009). Based on a total of 30 different preparation techniques applied by Jansen *et al*. (2008), the effect of chemical solutions and timing of treatment on pore size was examined for *P. wallichiana* and *Pinus radiata*. All SEM specimens were mounted on aluminium stubs using conductive carbon cement (Neubauer chemikaliën, Münster, Germany). Once dry, the mounted specimens were coated with platinum using an Emitech K550 sputter coater (Emitech Ltd, Ashford, UK) for 2 min, resulting in a ca. 10-nm-thick coating layer. Observations were carried out with a Hitachi cold-field emission SEM S-4700 (Hitachi High Technologies Corp., Tokyo, Japan) under 2 kV.

Table 1. List of the species studied with reference to their taxonomic family and origin; specimens in bold show pores in the torus of bordered pit pairs observed by electron microscopy

Family	Species	Authority	Origin and accession number	P_{50} (MPa) ± SE
Cephalotaxaceae	_Cephalotaxus fortunei_	Hook.	RBG Kew, 1969-16466	–7.21 ± 0.48
Cephalotaxaceae	**_Cephalotaxus harringtonii_**	**Knight ex J.Forbes**	**RBG Kew, 1969-16244**	**–7.21 ± 0.48**
Cupressaceae	_Callitris columellaris_^{a}	F.Muell.	University of Tasmania, Hobart	–15.79 ± 0.18
Cupressaceae	_Callitris gracilis_^{a}	R.T.Baker	University of Tasmania, Hobart	–12.26 ± 0.59
Cupressaceae	_Callitris preissii_^{a}	Miq.	University of Tasmania, Hobart	–14.96 ± 0.50
Cupressaceae	_Callitris rhomboidea_^{a}	R.Br.	University of Tasmania, Hobart	–9.60 ± 1.45
Cupressaceae	_Chamaecyparis obtusa_	Siebold & Zucc.	RBG Kew, 1969-10594	–3.70 ± 0.12
Cupressaceae	_Chamaecyparis pisifera_	(Siebold & Zucc.) Endl.	RBG Kew, 607-12-60702	–3.46 ± 0.21
Cupressaceae	_Cupressus dupreziana_	A.Camus	RBG Kew, 1970-6193	–10.29 ± 0.60
Cupressaceae	_Cupressus torulosa_	D.Don	RBG Kew, 1996-1799	–8.35 ± 0.60
Cupressaceae	_Metasequoia glyptostroboides_*	Hu & W.C.Cheng	RBG Kew, 1980-6256	–2.91 ± 0.13
Cupressaceae	_Platycladus orientalis_	(L.) Franco	RBG Kew, 1976-3574	–9.04 ± 0.45
Cupressaceae	**_Sequoia sempervirens_**	**Endl.**	**University of Bordeaux, Château du Haut-carré**	**–4.38 ± 0.17**
Cupressaceae	**_Sequoiadendron giganteum_**	**(Lindl.) J.Buchholz**	**University of Bordeaux, Château du Haut-carré**	**–3.79 ± 0.07**
Cupressaceae	_Taiwania cryptomerioides_	Hayata	RBG Kew, 1994-900	–3.38 ± 0.29
Cupressaceae	_Thuja plicata_*	Donn ex D.Don	RBG Kew, 1973-18600	–4.20 ± 0.13
Cupressaceae	_Thujopsis dolabrata_	Siebold & Zucc.	RBG Kew, 1969-16072	–5.63 ± 0.41
Cupressaceae	**_Xanthocyparis nootkatensis_**	**(D.Don) Farjon & D.K.Harder**	**RBG Kew, 1969-13806**	**–5.14 ± 0.25**
Pinaceae	**_Abies balsamea_*^{b}**	**(L.) Mill.**	**University of Alberta, Edmonton, Canada**	**–3.64 ± 0.34**
Pinaceae	_Cedrus atlantica_*	(Endl.) G.Manetti ex Carrière	RBG Kew, 2000-4686	–5.13 ± 0.08
Pinaceae	_Cedrus deodara_	Loudon	Clermont-Ferrand, France	–7.25 ± 0.41
Pinaceae	**_Larix decidua_***	**Mill.**	**RBG Kew, 1979-6300**	**–4.30 ± 0.37**
Pinaceae	**_Picea glauca_*^{b}**	**(Moench) Voss**	**University of Alberta, Edmonton, Canada**	**–4.35 ± 0.26**
Pinaceae	**_Picea mariana_*^{b}**	**(Mill.) BSP.**	**Edson, Canada**	**–5.21 ± 0.19**
Pinaceae	**_Pinus hartwegii_***	**Lindl.**	**RBG Kew, 1996-1016**	**–3.43 ± 0.18**
Pinaceae	**_Pinus nigra_***	**J.F.Arnold**	**RBG Kew, 1973-15503**	**–3.52**
Pinaceae	**_Pinus pinaster_***	**Aiton**	**Bordeaux, 503, 361, 441, 463B**	**–3.73 ± 0.07**
Pinaceae	**_Pinus radiate_**	**D.Don**	**University of Tasmania, Hobart**	**–4.38 ± 0.14**
Pinaceae	**_Pinus wallichiana_*^{c}**	**A.B.Jacks**	**RBG Kew, 1979-2373**	**–2.39**
Sciadopityaceae	_Sciadopitys verticillata_	Siebold & Zucc.	RBG Kew, 1979-48	–3.94 ± 0.13
Taxaceae	_Torreya californica_	Torr.	RBG Kew, 1969-14196	–6.39 ± 0.30
Taxaceae	_Torreya grandis_	Fortune ex. Lindl.	RBG Kew, 1973-20815	–4.69 ± 0.25
Taxaceae	_Torreya nucifera_	Siebold & Zucc.	RBG Kew, 1969-15523	–5.94 ± 0.30

Air-dried material was used for scanning electron microscopy (SEM); transmission electron microscopy (TEM) was based on air-dried material for most species, but on fresh material for species followed by an asterisk (*). Average P_{50} values are based on three to five specimens and correspond to the pressure inducing 50% loss of hydraulic conductance; $n = 1$ specimen for _P. nigra_ and _P. wallichiana_. ^{a}Material studied by Brodribb _et al_. (2010); ^{b}material studied by Hacke & Jansen (2009); ^{c}material studied by Jansen _et al_. (2008).

Transmission electron microscopy (TEM)

TEM was based on one wood sample per species, selecting the same branch that was also used for SEM. Air-dried wood from the two most recent growth rings was cut into 1 mm^3 blocks and dehydrated through a graded ethanol series. The ethanol was gradually replaced with LR White resin (London Resin Co, Reading, UK) over several days. The resin was polymerized in a Gallenkamp vacuum oven at 60 °C and 1000 mbar for 24 h. Embedded samples were trimmed with a Leica EM specimen trimmer (Leica Microsystems, Vienna, Austria) and sectioned on an ultramicrotome (Ultracut, Reichert-Jung, Austria). Transverse, ultra-thin sections were cut between 60 and 90 nm using a diamond knife, attached to Formvar (Agar Scientific, Stansted, UK) and 100 mesh copper grids, and stained with uranyl acetate and lead citrate using a Leica EM Stain Ultrostainer (Leica Microsystems). Observations were carried out with a JEOL JEM-1210 TEM (Jeol, Tokyo, Japan) at 80 kV accelerating voltage, and digital images were taken using a MegaView III camera (Soft Imaging System, Münster, Germany).

For 11 species (Table 1), TEM was applied to fresh material, which was cut into 1 mm^3 blocks and fixed overnight in Karnovsky's fixative at room temperature. After washing in a 0.05 M phosphate buffer, the specimens were postfixed in 1% buffered osmium tetroxide for 4 h at room temperature, and washed again. Further preparation followed the method given above.

Anatomical measurements

For each species a minimum of ca. 100 tori was observed using SEM, while the size of ultra-thin sections limited TEM observations to ca. 50 tori per species. SEM observations were mainly conducted on aspirated pit membranes at magnifications above 10 000. Both non-aspirated and aspirated pit membranes were seen with TEM, with higher frequencies of relaxed pit membranes in fresh material than air-dried wood.

Pit morphological features from earlywood tracheids were quantified for all 13 species with punctured tori. Pit membrane diameter (D_m), torus diameter (D_t) and pit aperture diameter (D_a) were measured at the widest point and in horizontal direction using SEM images. Pits with torus extensions (i.e. margo straps) were excluded from torus diameter measurements. Because of significant scaling between D_m, D_t and D_a (Hacke & Jansen 2009; Supporting Information Figure S2), a minimum of 15 aspirated pit membranes per species were measured, which allowed quantifying D_m, D_t and D_a on the same pit. Torus overlap (O) was defined following Delzon *et al*. (2010) as $(D_t - D_a)/D_t$, and as $(D_t - D_a)/(D_m - D_a)$ according to Hacke *et al*. (2004). The margo flexibility index ($F = (D_m - D_t)/D_t$) and valve effect ($V_{ef} = F \times O$) were estimated according to Delzon *et al*. (2010). The size of the pores associated with tori was consistently measured for a minimum of 25 pores per species. For most species, however, we measured more than 40 pores from ca. 20 pit membranes. For the *P. wallichiana* samples prepared according to Jansen *et al*. (2008), only conditions similar to 5 min of alcohol treatment were used to measure pore size.

Based on TEM images, the maximum margo thickness (M_t), the torus thickness (T_t) in the centre of the torus and the pit chamber depth (i.e. the maximum distance between overarching pit borders of a pit pair, D_p) were measured for all species with punctured tori except for *P. wallichiana* and *Sequoiadendron giganteum*. Average values for these TEM characteristics were determined based on a minimum of 10 measurements.

All anatomical measurements were conducted using ImageJ software (Rasband 1997–2011).

Xylem vulnerability to cavitation

To investigate intraspecific variation, vulnerability to cavitation was measured for three to five specimens per species. Except for the three species studied by Hacke & Jansen (2009; Table 1), vulnerability curves were based on the cavitron technique as described previously (Cochard 2002; Cochard *et al*. 2005; Delzon *et al*. 2010). Measurements were performed at the high-throughput phenotyping platform for hydraulic traits (CaviPlace, University of Bordeaux, Talence, France) using a custom-built honeycomb rotor (Precis 2000, Bordeaux, France) mounted on a Sorvall RC5 ultracentrifuge (Fisher Scientific, Schwerte, Germany). Samples were kept refrigerated and vulnerability to cavitation was determined within 2 weeks of collection. All samples were debarked to avoid resin exudation, re-cut under water to a standard length of 27 cm, and both ends were trimmed with a fresh razor blade to obtain perfectly smooth surfaces with open tracheids. A solution of ultra-pure and degassed water including 10 mM KCl and 1 mM $CaCl_2$ was used as reference solution for hydraulic measurements. After measuring the maximum hydraulic conductance under low (i.e. close to zero) xylem pressure (P), the rotation speed of the centrifuge was gradually increased by 0.5 or 1 MPa to determine the percentage loss of hydraulic conductance (PLC). The rotor velocity was monitored using an electronic tachymeter (A2108-LSR232; Compact Inst, Bolton, UK) with a 10 r.p.m. resolution, and the xylem pressure was adjusted to ±0.02 MPa. We used Cavi_soft software (version 1.5, University of Bordeaux) for conductance measurements and the computation of all vulnerability curves, which were adjusted according to Pammenter and Vander Willigen (1998). The P_{50} value was defined as the pressure corresponding to 50% PLC and averaged for each species. Similarly, P_{12} was defined as the pressure equivalent to 12% PLC, which corresponds to air entry in the xylem. S_{50} was defined as the slope of the vulnerability curve at the inflexion point (Pammenter & Vander Willigen 1998), which corresponds to the speed of embolism in the xylem system per unit of pressure (% MPa^{-1}).

The theoretical pressure gradient (ΔP, in MPa) required to pull an air bubble through the pore of a pit membrane was calculated based on the Young–Laplace equation as $\Delta P = 4\,(\tau \cos\theta / D)$, where D (nm) represents the diameter of the pit membrane pore and τ (N m^{-1}) is the surface tension of water. The contact angle (θ) between the air-water-pit membrane interface was assumed to be 0°.

Statistical analysis

Statistical differences between species with punctured tori ($n = 13$) and non-punctured tori ($n = 20$) were inferred using the following mixed model:

$$\boldsymbol{y} = \boldsymbol{X\beta} + \boldsymbol{Z\gamma} + \boldsymbol{\varepsilon}$$

$\boldsymbol{y}$ is the observation vector (here P_{50} and S_{50}). $\boldsymbol{X}$ represents a design matrix linking the observation to fixed effects and $\boldsymbol{\beta}$ is a vector of the fixed effect (here, *torus anatomy* with two levels 'punctured' and 'non-punctured tori'). $\boldsymbol{Z}$ is a random effect matrix linking observations to random effects and $\boldsymbol{\gamma}$ is a random effects vector (here, *family* with five levels and *genus* nested within *family* with one to five levels). At first, we ran the fixed part of this model to assess if there was an effect of torus anatomy on P_{50} and S_{50}. Afterwards, the full model was run to consider the putative phylogenetic autocorrelation between species (Chave *et al*. 2009). Differences were considered statistically significant at $P \leq 0.05$.

Classical linear regression analyses were used to determine the relationship between (1) torus capillary-seeding and resistance to cavitation; (2) pit dimensions (D_a, D_t, D_m); (3) pore diameter in tori and torus thickness; and (4) pit functional traits (O, F, V_{ef}).

Statistical analyses were performed using SAS software (SAS 9.2; SAS Institute, Cary, NC, USA).

RESULTS

The anatomy of punctured tori

Torus-margo pit membranes were found in all species studied. The torus could be distinguished from the margo due to its non-porosity and high electron density as seen with the SEM and TEM, respectively (Figs 1 & 2). Punctured tori were observed in 13 species using SEM (Table 1; Fig. 1b–j), while all other species studied showed tori without distinct pores (Fig. 1a). Punctured tori were consistently present in the two specimens of *P. hartwegii* and the four trees of *P. pinaster* studied.

The size of the pores varied from 12 to 144 nm, with a mean diameter of 49 (±9) nm (±SD) based on SEM

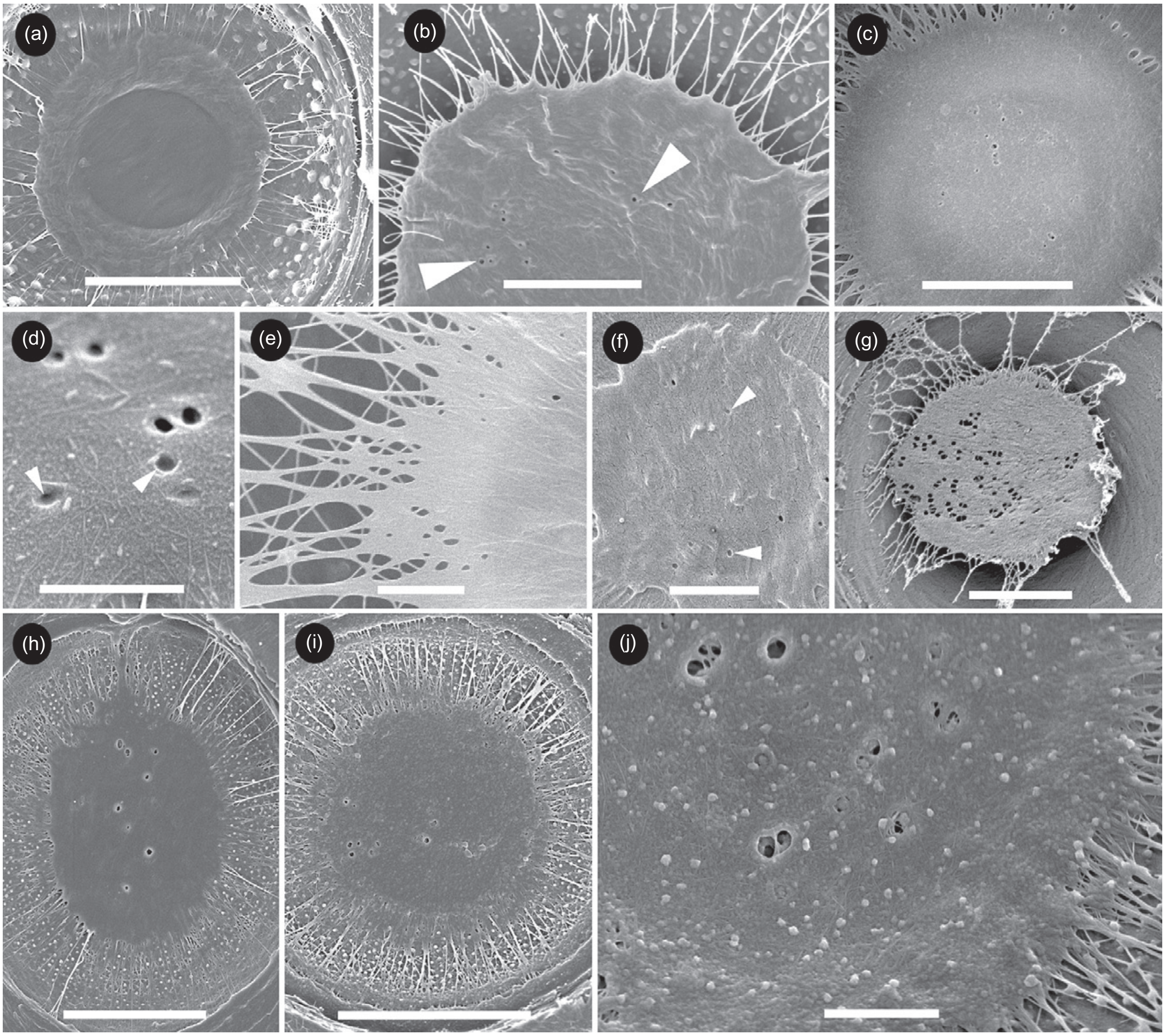

Figure 1. Scanning electron microscope images of bordered pit membranes in conifer tracheids showing the ultrastructure of the torus. (a) *Pinus radiata*, aspirated pit membrane, the outline of the inner pit aperture, which has a smaller diameter than the torus, can be seen through the torus, distinct warts occur on the surface of the pit border, scale bar = 5 μm; (b) *Pinus pinaster*, arrowheads indicate several pores in the torus, scale bar = 2 μm; (c) *Cephalotaxus harringtonii*, detail of torus with minute pores, scale bar = 2 μm; (d) *Picea mariana*, detail of torus with shallow (arrowheads) and deep pores, scale bar = 500 nm; (e) *Torreya californica*, detail of torus and margo, the pores occurring on the torus-margo border are interpreted as margo pores and not as plasmodesmatal pores, scale bar = 500 nm; (f) *Pinus wallichiana*, torus detail of oven dried (100 °C) sample, some of the pores appear superficial and partly filled with material (arrowheads), scale bar = 2 μm; (g) *P. wallichiana*, sample after critical point drying and treatment with 100% ethanol, which resulted in an increased pore size and reduced microfibril network of the margo, scale bar = 2.5 μm; (h) *Sequoia sempervirens*, aspirated pit membrane with punctured torus, scale bar = 5 μm; (i) *Sequoiadendron giganteum*, overview of a punctured torus, scale bar = 5 μm; (j) *S. giganteum*, detail of pores showing different levels of penetration into the torus, scale bar = 1 μm.

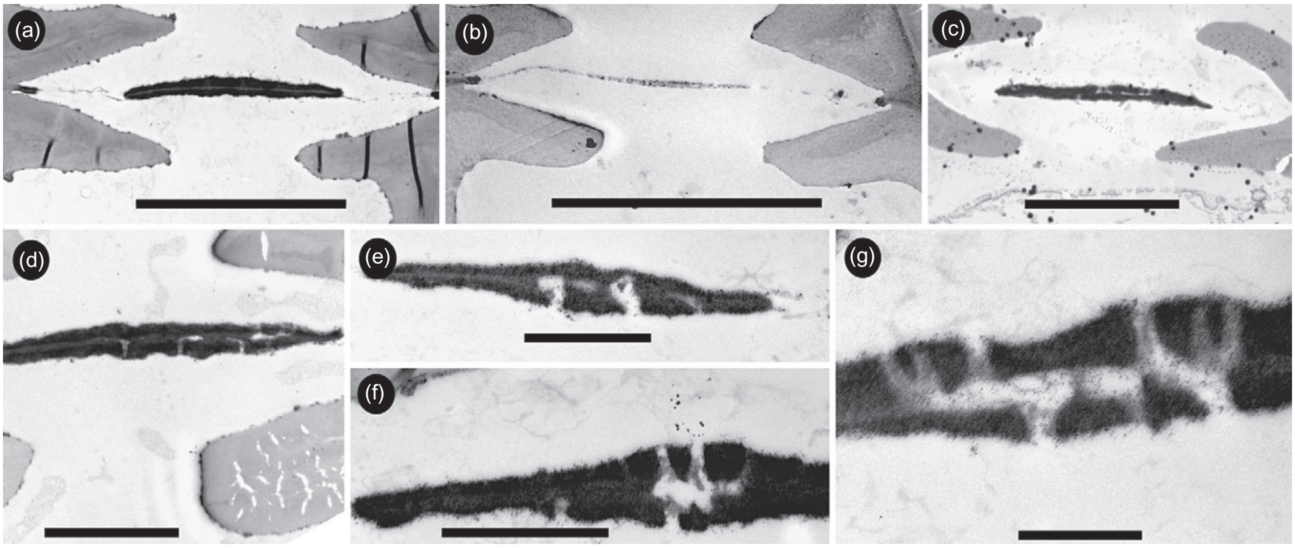

Figure 2. Transmission electron microscope images of bordered pit membranes in conifer tracheids showing details of the central torus and plasmodesmatal channels. (a) *Pinus hartwegii*, pit membrane showing a non-punctured, electron dense torus, thin margo and electron dense pit membrane annulus near the pit border, scale bar = 5 μm; (b) *Metasequoia glyptostroboides*, thin pit membrane consisting of a margo and indistinct, thin torus, scale bar = 5 μm; (c) *Larix decidua*, torus with minute pores, scale bar = 5 μm; (d) *Pinus pinaster*, detail of torus with several plasmodesmatal channels, scale bar = 2 μm; (e) *P. hartwegii*, two distinct plasmodesmatal channels seemingly terminating at the middle lamella, a third, indistinct pore can be seen on the right, scale bar = 1 μm; (f) *P. hartwegii*, pores piercing the entire torus and sharing a single median cavity, scale bar = 1 μm; (g) *P. hartwegii*, various plasmodesmatal pores with a typically branched pattern share a single median cavity and give the torus a sieve-like, permeable appearance, scale bar = 500 nm.

(Supporting Information Table S1). Treatment with alcohol and other dissolving solutions had a clear effect on the size of the pores in *P. wallichiana* (Fig. 1f,g). The average pore size in this species (61 nm ± 27) increased substantially after the following treatments: 85 (±42) nm (formalin-acetic-alcohol treatment), 135 (±57) nm (100% ethanol in combination with critical point drying; Fig. 1g), 116 (±42) nm (glacial acetic acid) and 100 (±17) nm (oven drying at 100 °C; Fig. 1f). However, no significant difference was found with respect to the pore size in *P. radiata* when comparing no alcohol treatment with 5 min of ethanol treatment. The only morphological difference was that pores in SEM material not treated with alcohol showed a circular depression with a slightly raised area in the centre, which was not seen after alcohol treatment (images not shown).

No difference was found in the occurrence of punctured tori between ray tracheid to longitudinal tracheid pit pairs and longitudinal tracheid bordered pit pairs. Overall, the frequency of the pores was low and rarely exceeded more than 10% of the pits. The highest frequencies were counted in *P. hartwegii*, in which tori with pores were found in 31% of the pits observed. The shape of the pores was usually round. Some pores appeared superficial and partly filled with material, while others penetrated more deeply into the torus (Fig. 1d,f,j). They were distributed across the entire torus, with similar frequency in the centre and peripheral areas of the torus. However, in most cases the pores were characteristically grouped in small pairs of two or more (Fig. 1b–j).

In some species, solitary pores near the edge of the torus as seen with SEM were not interpreted as plasmodesmatal pores because of their similarity in size and morphology to margo pores (Fig. 1e). The largest margo pores varied from 330 to 1060 nm. Margo pores near the periphery of the torus were especially common in species with torus extensions (*Cupressus dupreziana*, *Cupressus torulosa*, *Sequoia sempervirens*), and in species with a relatively thin torus (*Metasequoia glyptostroboides*, *Thujopsis dolabrata* and *Torreya grandis*; Fig. 2b). Minute pores (generally < 50 nm) could also be seen using SEM and TEM in the central part of the torus in the latter three species, which showed an average torus thickness around 100 nm as compared with a mean torus thickness of 503 nm for species with punctured tori (Fig. 5). Not only the size of the torus pores in *M. glyptostroboides*, *T. dolabrata* and *T. grandis*, but also their non-grouped distribution suggested that these pores did not represent plasmodesmatal pores, but were due to the thin torus nature.

TEM observations demonstrated the occurrence of punctured tori in six species, in which this feature was also seen with SEM (Fig. 2c–g). However, no pores could be detected with TEM in *Cephalotaxus harringtonia*, *Chamaecyparis nootkatensis*, *Picea glauca*, *P. wallichiana*, *P. radiata* and *S. sempervirens*, which showed pores based on SEM (Fig. 1c,f,g). TEM measurements of the pore size were larger than those based on SEM, but within the same order of magnitude. The average TEM pore size was 64 (±10) nm (±SD), and the largest pore measured based on TEM was 150 nm in *Larix decidua*. Most pores could not be seen to extend through the complete torus, but were limited to one torus pad and gave the impression of terminating in a cavity near the middle lamella (Fig. 2c–e). However, pores were occasionally seen to traverse the entire torus (Fig. 2f,g), and TEM confirmed that the channels were usually arranged in a branched pattern, with several pores connected laterally to each other via an extensive median cavity at the level of the middle lamella (Fig. 2f,g). The branched channels occasionally resulted in a sieve-like appearance of the torus (Fig. 2g).

Xylem vulnerability to cavitation

P_{50} values varied from –15.79 to –2.39 MPa among the species studied (Table 1). There was a significant difference ($P = 0.01$) in vulnerability to cavitation (P_{50}) between species with and without punctured tori: species with punctured tori were less cavitation resistant than species with no plasmodesmatal pores associated with their tori, with average P_{50} values of –4.3 and –7.2 MPa, respectively (Fig. 3). Similarly, we found that species with punctured tori have a greater S_{50} compared with species without punctured tori (Supporting Information Figure S1; $P < 0.0001$), and that this trend remained significant with control for taxonomy ($P = 0.024$). However, there was no statistical significance when considering the taxonomic influence on the difference in P_{50} between species with and without punctured tori ($P = 0.21$).

The air-seeding pressures estimated using the largest margo pores varied from 0.27 to 0.88 MPa and were 10 times lower in absolute value than the measured air-seeding pressure (P_{50}). By contrast, the air-seeding pressures based on the SEM size of plasmodesmatal pores in tori were of the same order of magnitude than the measured air-seeding pressures, varying from 2.02 to 4.16 MPa. However, there were weak correlations between P_{50} values derived from vulnerability curves and the theoretical air-seeding pressures based on the maximum and average SEM pore sizes, which corresponded to the torus capillary-seeding pressures (Fig. 4a). Torus capillary-seeding pressures as based on the average SEM pore sizes were lower in absolute value than the P_{50} values in all species. There was a significant correlation between the P_{12} values and the torus capillary-seeding pressure based on the maximum SEM pore size (Fig. 4b). Weak correlations were found when plotting P_{50} versus air-seeding based on average SEM pore size ($P = 0.064$; Fig. 4a), and P_{12} values versus air-seeding pressures derived from average SEM pore sizes ($P = 0.074$; Fig. 4b).

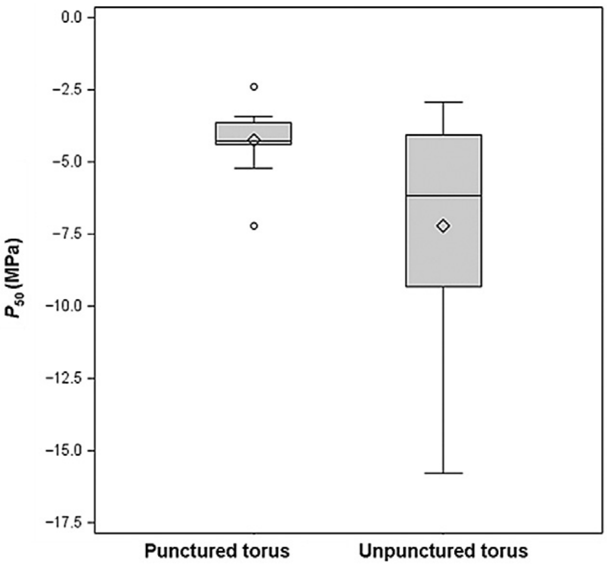

Figure 3. Box plot illustrating a significant difference ($P = 0.01$) in vulnerability to xylem cavitation (P_{50}, i.e. the pressure required to induce 50% loss of hydraulic conductance) between species with punctured tori ($n = 13$) and non-punctured tori ($n = 20$). This trend is not significant ($P = 0.21$) when including taxonomy based on a mixed model (see Materials and methods for details).

A strong allometry was found between D_m, D_t and D_a for species with punctured tori (Supporting Information Figure S2) with high coefficients of determination (Pearson correlation coefficients $R = 0.93$ for D_m versus D_t; $R = 0.88$ for D_m versus D_a; $R = 0.87$ for D_t versus D_a) and high significance ($P < 0.0001$). The slope of the regression lines was more or less similar for D_m versus D_t and D_t versus D_a (0.55 and 0.5, respectively), but lower for D_m versus D_a (0.30). Across the species with punctured tori, D_m, D_t and D_a decreased with increasing resistance to cavitation. However, only D_t showed a significant correlation with P_{50} (Pearson correlation = 0.63, $P = 0.02$).

Pit chamber depth (D_p), margo thickness (M_t) and torus thickness (T_t) showed no correlation with P_{50}. Interestingly, torus thickness (T_t) was positively correlated with the maximum diameter of plasmodesmatal pores, but not with the average pore diameter based on SEM (Fig. 5). P_{50} values were not correlated with valve effect (V_{ef}) and torus overlap (O), but weakly correlated with margo flexibility (F) (Fig. 6).

DISCUSSION

Our results suggest that torus capillary-seeding is a likely hypothesis in some conifers. Indeed, the size of the torus pores corresponds to the pressure inducing cavitation event and particularly to the xylem air-entry point (P_{12}, Fig. 4b): the larger the pore diameter, the less cavitation resistant the species (Jarbeau, Ewers & Davis 1995; Choat *et al.* 2008). Because air-seeding will always occur at the largest pore first, maximum pore sizes should in theory correlate more strongly with air-seeding thresholds than average values (Choat *et al.* 2003; Jansen *et al.* 2009). It is surprising that in our dataset no significant correlations are found between cavitation resistance with torus overlap, torus thickness, and the torus to aperture ratio, although measurements obtained for pit membrane diameter (D_m), aperture diameter (D_a) and especially torus diameter (D_t) are consistent with previous hypotheses explaining cavitation resistance in conifers (Hacke & Jansen 2009; Delzon *et al.* 2010; Pittermann *et al.* 2010). This finding suggests that the pores associated with tori are likely to explain variation in cavitation

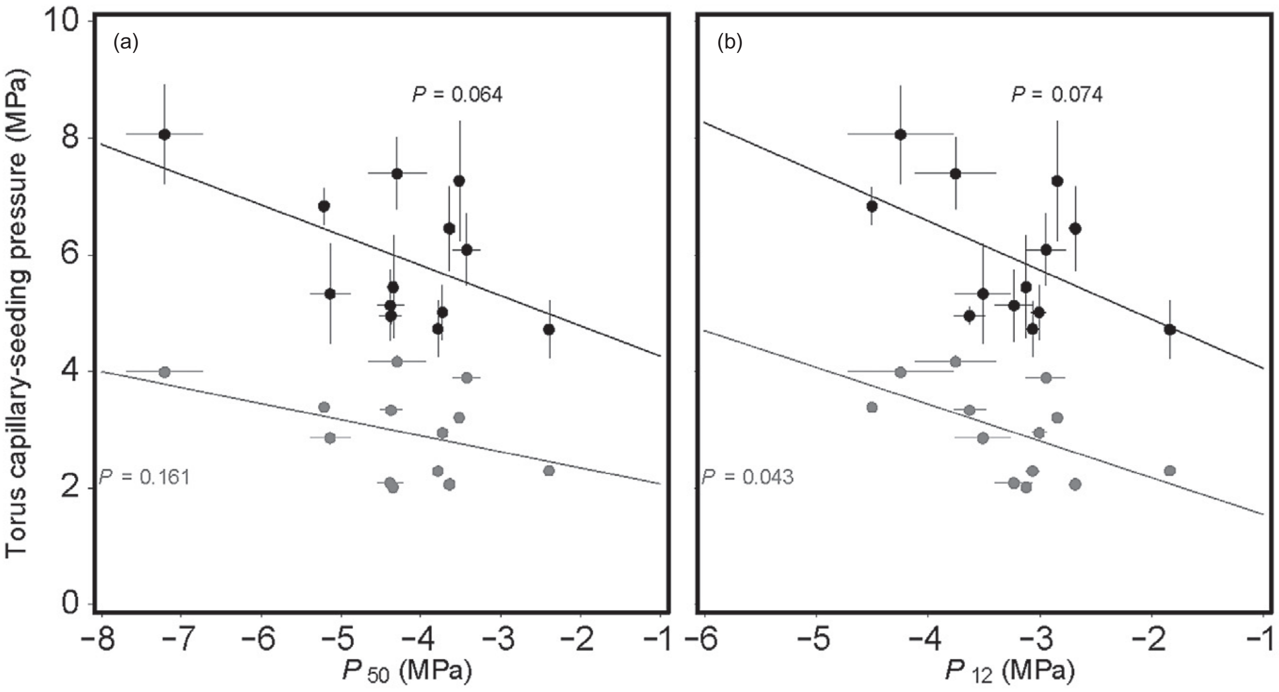

Figure 4. Xylem vulnerability to cavitation quantified as (a) P_{50} and (b) P_{12} (i.e. the pressure corresponding to 50 and 12% loss of hydraulic conductance, respectively) versus the torus capillary-seeding pressure (MPa). The latter was calculated based on the average (black circles) and maximum (grey circles) scanning electron microscopy (SEM) pore size ($n \geq 25$) for 13 conifer species with punctured tori. Data represent average values per species ± SE. A significant relationship was found between P_{12} values and the torus capillary-seeding pressures based on the maximum pore size, while non-significant correlations were found when analysing P_{50} values and torus capillary-seeding pressures based on the average and maximum pore size.

resistance equally as well as other pit morphological features.

Correlations between theoretical and measured air-seeding pressures among the 13 species with punctured tori are weak (Fig. 4) and absolute pore diameter measurements based on SEM should be interpreted with caution for various reasons. At first, only pores that traverse the torus are potential places for air-seeding. Although superficial pores can be distinguished from deeper ones in most cases (Fig. 1d,j), SEM does not allow the distinction between pores that completely pierce the torus from those that are limited to one torus pad. Our TEM observations illustrate that at least a few pores in each species with punctured tori completely traverse the torus (Fig. 2f,g). Careful TEM observation of serial sections would be most useful to quantify the number of pores running from one end of the torus to the other. Secondly, the diameter of the pore measured on the outermost surface of the torus may not correspond to the minimum diameter of the total channel, which determines at what pressure difference the air-water interface is pulled through the pore (Sperry & Tyree 1988; Sperry *et al.* 1996). Estimating the diameter of a pore at nanometer scale is not always free from bias, because the exact outline of the pore may not be clearly visible, even when using high magnifications and optimal contrast conditions with a cold-field emission SEM. Furthermore, the thickness of the coating layer (ca. 10 nm) could have an effect on the actual pore size in pit membranes (Jansen *et al.* 2008). Finally, pore size measurements based on SEM have been shown to offer relative estimates of air-seeding thresholds (Jansen *et al.* 2009) and should be complemented with other techniques such as air injection or particle perfusion experiments (Choat *et al.* 2004, 2005).

The plasmodesmatal nature of the pores can be confirmed based on two arguments: (1) the average pore size corresponds with the ca. 50 nm diameter of plasmodesmata (Murmanis & Sachs 1969; Roberts 2005; Bell & Oparka 2011); and (2) their grouped distribution and branched pattern reflect the characteristically uneven and branched arrangement of secondary plasmodesmata (Rabaey *et al.* 2008). Variation in average pore size between SEM and TEM (51 and 64 nm, respectively) is likely due to differences in sample preparation and observation. While detailed surface views of pores are possible with a field-emission SEM, ultra-thin sections prepared for TEM may show pores in an oblique way with more indistinct contours than SEM. Therefore, we believe that pore size measurements based on SEM are more accurate than TEM. The increase in pore size in *P. wallichiana* after treatment with various chemicals corresponds with earlier observations by Fujikawa & Ishida (1972). As illustrated in Fig. 5, the maximum pore diameter correlates positively with the torus thickness, which is contradictory to earlier findings in angiosperms (Jansen *et al.* 2009): larger pores are more

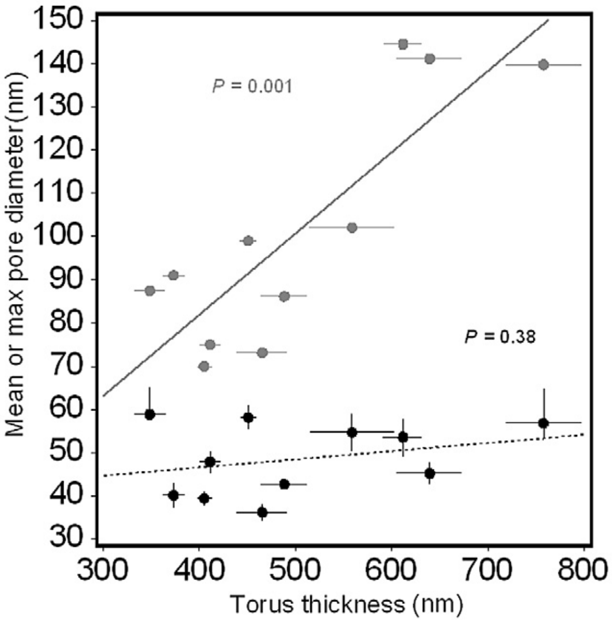

Figure 5. The ratio torus thickness to plasmodesmatal pore diameter showed a significant correlation for the maximum pore diameter, but not for the average pore diameter values for 11 species with punctured tori. Torus thickness was based on transmission electron microscopy (TEM) observations, while dimensions of pores in tori were measured using scanning electron microscopy (SEM). Data represent average values per species ± SE.

likely to occur in thin, flimsy pit membranes than in thick and solid pit membranes.

Given the plasmodesmatal origin of the pores associated with tori, it is not surprising that there is a relatively constant average pore size. Therefore, we believe that it is unlikely that plasmodesmatal pores with actual pore sizes below 30 nm (corresponding to air-seeding below 10 MPa) occur. Thus, rather limited variation in P_{50} values would be found among species with punctured tori, but more variation in cavitation resistance and more negative P_{50} values among species without punctured tori. This is supported by the finding that P_{50} values are more variable and higher in absolute value in species without punctured tori compared with species with punctured tori (Fig. 3). Likewise, the distribution of punctured tori may explain why a large and ecologically diverse genus such as *Pinus* shows relatively little variation with respect to P_{50} values, which generally ranges from −2.5 to −4.5 MPa, although more negative P_{50} values have been recorded in few species (Sperry & Tyree 1990; Piñol & Sala 2000; Hacke *et al*. 2004; Martínez-Vilalta, Sala & Piñol 2004; Martínez-Vilalta *et al*. 2009; Lamy *et al*. 2011). As there seems to be no true selective advantage of having punctured tori, one may also speculate that this phenomenon is tolerated in some conifer species with a particular life history. Incomplete plasmodesmatal sealing of the torus could be acceptable for instance in fast-growing conifers such as *Sequoia*, *Sequoiadendron* and various Pinaceae. Further research is clearly needed to consider possible trade-offs between species with punctured tori and habitat, growth rate and cavitation resistance to drought.

The most likely explanation why pores could not be detected with TEM in five species in which punctured tori were seen with SEM, is that punctured tori are only occasionally present and SEM allows the observation of a higher number of tori than TEM. In addition, TEM sections represent only small fragments of the entire torus, and even if pores would be present, it is possible that they cannot be seen in the ultra-thin sections either because of their arrangement in small groups, or because the pores are narrower than the 60–90 nm thickness of TEM sections. The latter may also explain why most pores seen in TEM sections are not completely open and free from matrix material (Fig. 2e–g). Again, careful examination of serial sections might be required to detect plasmodesmatal pores with TEM.

Based on the limited number of 33 species studied, punctured tori appear to be relatively common across conifer taxa and are not limited to particular taxonomic families or genera. It is possible that the occasional retention of plasmodesmatal pores in some conifer taxa reflects differences in the chemical composition of conifer tori. As far as we know, however, gymnosperm tori show an overall similarity in chemical composition and mainly consist of pectins (Bauch & Berndt 1973; Imamura, Harada & Saiki 1974; Hafrén, Daniel & Westmark 2000; Putoczki *et al*. 2008; Kim *et al*. 2011). Alternatively, the

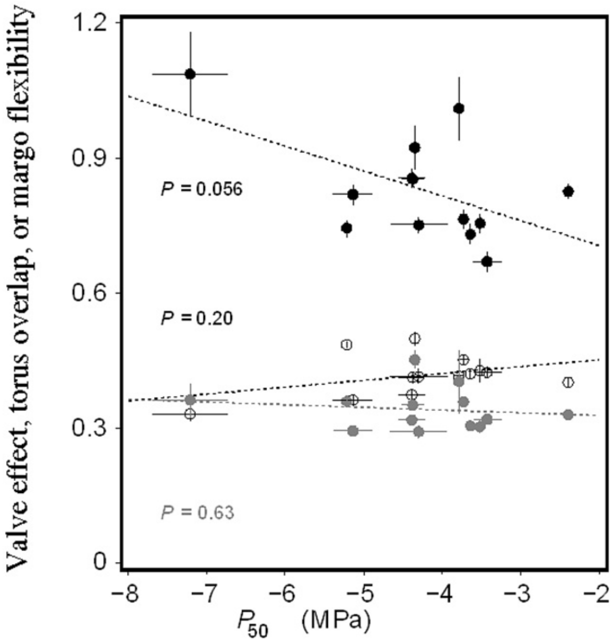

Figure 6. No significant relationship was found between P_{50} versus valve effect (V_{ef}, grey symbols) sensu Delzon *et al*. (2010), torus overlap (*O*, blank circles), and margo flexibility (*F*, black dots) for 13 species with punctured tori. Data represent average values per species ± SE. Furthermore, no significant relationship was found between P_{50} and torus overlap sensu Hacke *et al*. (2004) ($P = 0.12$; data not shown).

presence or absence of plasmodesmatal pores could be explained by differences in torus development among conifers. Plasmodesmata seem very common in developing pit membranes of conifer tracheids (Murmanis & Sachs 1969; Thomas 1969; Fengel 1972; Fujikawa & Ishida 1972; Dute 1994; Dute *et al*. 2008), although it is unclear whether their frequency in developing tori corresponds with similar frequencies of punctured tori in mature pit membranes. While secondary plasmodesmata associated with tori appear during the final stages of cell differentiation in *A. firma* (Pinaceae) and *M. glyptostroboides* (Cupressaceae), they are only retained in mature pit membranes of *A. firma*. In contrast, autolytic enzymes remove matrix from the torus in *M. glyptostroboides*, which results in a loss of the plasmodesmatal channels and rearrangement of microfibrils (Dute 1994; Dute *et al*. 2008). Whether or not plasmodesmatal openings remain present in the fully developed torus after autolysis may thus depend on the degree and conditions of the autolysis. Clearly, more developmental research will be needed to test this idea.

In conclusion, this study suggests that the torus in conifer pit membranes is not always as airtight as previously thought. While air-seeding through pores in the torus does not represent the only and universal mechanism for drought-induced cavitation in conifers, there is preliminary evidence indicating that plasmodesmatal pores could contribute to air-seeding, supporting the torus capillary-seeding hypothesis. In species without punctured tori, cavitation might occur between the torus and the outer pit chamber wall when the torus is not tightly sealed against the pit border (seal capillary-seeding). This finding will hopefully encourage further work on the structural basis behind cavitation resistance in woody plants, which will also be useful for untying the genetic mechanisms of drought resistance in plants.

ACKNOWLEDGMENTS

We thank Tony Kirkham (RBG Kew) for permission to collect samples from the living collections in Kew. Tim Brodribb (University of Tasmania) and Uwe Hacke (University of Alberta) are acknowledged for providing wood samples. Financial support to Kew and Bordeaux was provided by an International Joint grant from the Royal Society (UK). S.J. acknowledges a 'Juniorprofessorenprogramm' grant from the Ministry of Science, Research, and the Arts of Baden-Wurttemberg (Germany). Funding to S.D. and J.-B.L. was provided by grants from INRA-Project Innovant and a PhD grant from INRA-Région Auvergne, respectively. A mobility grant to J.-B.L. was provided by INRA (France).

REFERENCES

Bailey I.W. (1913) The preservative treatment of wood. II. The structure of the pit membranes in the tracheids of conifers and their relation to the penetration of gases, liquids, and finely divided solids into green and seasoned wood. *Forestry Quarterly* **11,** 12–20.

Bailey I.W. (1916) The structure of bordered pits of conifers and its bearing upon the tension hypothesis of the ascent of sap in plants. *Botanical Gazette* **62,** 133–142.

Bao F.C., Lu J.X. & Zhao Y. (2001) Effect of bordered pit torus position on permeability in Chinese yezo spruce. *Wood and Fiber Science* **33,** 193–199.

Bauch J. & Berndt H. (1973) Variability of the chemical composition of pit membranes in bordered pits of gymnosperms. *Wood Science and Technology* **7,** 6–19.

Bauch J., Schultze R. & Liese W. (1972) Morphological variability of bordered pit membranes in gymnosperms. *Wood Science and Technology* **6,** 165–184.

Bell K. & Oparka K. (2011) Imaging plasmodesmata. *Protoplasma* **248,** 9–25.

Brodribb T.J., Bowman D.J.M., Nichols S., Delzon S. & Burlett R. (2010) Xylem function and growth rate interact to determine recovery rates after exposure to extreme water deficit. *New Phytologist* **188,** 533–542.

Chave J., Coomes D., Jansen S., Lewis S., Swenson N. & Zanne A. (2009) Towards a worldwide wood economics spectrum. *Ecology Letters* **12,** 351–366.

Choat B., Ball M., Luly J. & Holtum J. (2003) Pit membrane porosity and water stress-induced cavitation in four co-existing dry rainforest tree species. *Plant Physiology* **131,** 41–48.

Choat B., Jansen S., Zwieniecki M.A., Smets E. & Holbrook N.M. (2004) Changes in pit membrane porosity due to deflection and stretching: the role of vestured pits. *Journal of Experimental Botany* **55,** 1569–1575.

Choat B., Lahr E.C., Melcher P.J., Zwieniecki M.A. & Holbrook N.M. (2005) The spatial pattern of air seeding thresholds in mature sugar maple trees. *Plant, Cell & Environment* **28,** 1082–1089.

Choat B., Cobb A. & Jansen S. (2008) Structure and function of bordered pits: new discoveries and impacts on whole plant hydraulic function. *New Phytologist* **177,** 608–626.

Cochard H. (2002) A technique for measuring xylem hydraulic conductance under high negative pressures. *Plant, Cell & Environment* **25,** 815–819.

Cochard H., Damour G., Bodet C., Tharwat I., Poirier M. & Ameglio T. (2005) Evaluation of a new centrifuge technique for rapid generation of xylem vulnerability curves. *Physiologia Plantarum* **124,** 410–418.

Cochard H., Hölttä T., Herbette S., Delzon S. & Mencuccini M. (2009) New insights into the mechanisms of water-stress-induced cavitation in conifers. *Plant Physiology* **151,** 949–954.

Comstock G.L. & Côté W.A. (1968) Factors affecting permeability and pit aspiration in coniferous wood. *Wood Science and Technology* **2,** 279–291.

Delzon S., Douthe C., Sala A. & Cochard H. (2010) Mechanism of water-stress induced cavitation in conifers: bordered pit structure and function support the hypothesis of seal capillary-seeding. *Plant, Cell & Environment* **33,** 2101–2111.

Domec J.-C., Lachenbruch B., Meinzer F.C., Woodruff D.R., Warren J.M. & McCulloh K.A. (2008) Maximum height in a conifer is associated with conflicting requirements for xylem design. *Proceedings of the National Academy of Sciences of the United States of America* **105,** 12069–12074.

Dute R.R. (1994) Pit membrane structure and development in *Ginkgo biloba*. *International Association of Wood Anatomists Journal* **15,** 75–90.

Dute R., Hagler L. & Black A. (2008) Comparative development of intertracheary pit membranes in *Abies firma* and *Metasequoia glyptostroboides*. *International Association of Wood Anatomists Journal* **29,** 277–289.

Fengel D. (1972) Structure and function of the membrane in softwood bordered pits. *Holzforschung* **26,** 1–9.

Flynn K.A. (1995) A review of the permeability, fluid-flow, and anatomy of Spruce (*Picea* spp.). *Wood and Fiber Science* **27,** 278–284.

Fujikawa S. & Ishida S. (1972) Study on the pit of wood cells using scanning electron microscopy. 3. Structural variation of bordered pit membrane on the radial wall between tracheids in Pinaceae species. *Mokuzai Gakkaishi* **18,** 477–483.

Gortan E., Nardini A., Salleo S. & Jansen S. (2011) Pit membrane chemistry influences the magnitude of ion-mediated enhancement of xylem hydraulic conductivity in four Lauraceae. *Tree Physiology* **31,** 48–58.

Hacke U.G. & Jansen S. (2009) Embolism resistance of three boreal conifer species varies with pit structure. *New Phytologist* **182,** 675–686.

Hacke U.G., Sperry J.S. & Pittermann J. (2004) Analysis of circular bordered pit function – II. Gymnosperm tracheids with torus-margo pit membranes. *American Journal of Botany* **91,** 386–400.

Hafrén J., Daniel G. & Westmark U. (2000) The distribution of acidic and esterified pectin in cambium, developing xylem and mature xylem of *Pinus sylvestris*. *International Association of Wood Anatomists Journal* **21,** 157–168.

Hart C.A. & Thomas R.J. (1967) Mechanism of bordered pit aspiration as caused by capillarity. *Forest Products Journal* **17,** 61–68.

Imamura Y., Harada H. & Saiki H. (1974) Embedding substances of pit membranes in softwood tracheids and their degradation by enzymes. *Wood Science and Technology* **7,** 189–205.

Jansen S., Pletsers A. & Sano Y. (2008) The effect of preparation techniques on SEM-imaging of pit membranes. *International Association of Wood Anatomists Journal* **29,** 161–178.

Jansen S., Choat B. & Pletsers A. (2009) Morphological variation of intervessel pit membranes and implications to xylem function in angiosperms. *American Journal of Botany* **96,** 409–419.

Jarbeau J.A., Ewers F.W. & Davis S.D. (1995) The mechanism of water-stress-induced embolism in two species of chaparral shrubs. *Plant, Cell & Environment* **18,** 189–196.

Kim J.S., Awano T., Yoshinaga A. & Takabe K. (2011) Temporal and spatial diversities of the immunolabelling of mannan and xylan polysaccharides in differentiating earlywood ray cells and pits of *Cryptomeria japonica*. *Planta* **233,** 109–122.

Lamy J.-B., Bouffier L., Burlett R., Plomion C., Cochard H. & Delzon S. (2011) Uniform selection as a primary force reducing population genetic differentiation of cavitation resistance across a species range. *PLoS One* **6,** e23476.

Liese W. (1965) The fine structure of bordered pits in softwoods. In *Cellular Ultrastructure of Woody Plants* (ed. W.A. Coté), pp. 271–290. Syracuse University Press, New York, USA.

Liese W. & Bauch J. (1967) On the closure of bordered pits in conifers. *Wood Science and Technology* **1,** 1–13.

Liese W. & Johann I. (1954) Elektronenmikroscopische Beobachtungen über eine besondere Feinstruktur der verholzten Zellwand bei einigen Coniferen. *Planta* **44,** 269–285.

Maherali H., Pockman W.T. & Jackson R.B. (2004) Adaptive variation in the vulnerability of woody plants to xylem cavitation. *Ecology* **85,** 2184–2199.

Martínez-Vilalta J., Sala A. & Piñol J. (2004) The hydraulic architecture of Pinaceae – a review. *Plant Ecology* **171,** 3–13.

Martínez-Vilalta J., Cochard H., Mencuccini M., *et al.* (2009) Hydraulic adjustment of Scots pine across Europe. *New Phytologist* **184,** 353–364.

Murmanis L. & Sachs I.B. (1969) Seasonal development of secondary xylem in *Pinus strobus* L. *Wood Science and Technology* **3,** 177–193.

Pammenter N.W. & Vander Willigen C. (1998) A mathematical and statistical analysis of the curves illustrating vulnerability of xylem to cavitation. *Tree Physiology* **18,** 589–593.

Panshin A.J. & De Zeeuw C. (1980) *Textbook of Wood Technology*. McGraw-Hill, New York, USA.

Piñol J. & Sala A. (2000) Ecological implications of xylem embolism for several Pinaceae in the Pacific Northern USA. *Functional Ecology* **14,** 538–545.

Pittermann J. (2010) The evolution of water transport in plants: an integrated approach. *Geobiology* **8,** 112–139.

Pittermann J., Sperry J.S., Hacke U.G., Wheeler J.K. & Sikkema E.H. (2005) The torus-margo pit valve makes conifers hydraulically competitive with angiosperms. *Science* **310,** 1924.

Pittermann J., Choat B., Jansen S., Stuart S., Lynn L. & Dawson T. (2010) The relationships between cavitation safety and hydraulic efficiency in the pit membranes of conifers belonging to the Cupressaceae: the evolution of form and function. *Plant Physiology* **153,** 1919–1931.

Putoczki T.L., Gerrard J.A., Butterfield B.G. & Jackson S.L. (2008) The distribution of un-esterified and methyl-esterified pectic polysaccharides in *Pinus radiata*. *International Association of Wood Anatomists Journal* **29,** 115–127.

Rabaey D., Lens F., Huysmans S., Smets E. & Jansen S. (2008) The ultrastructure and development of pit membranes with plasmodesmata associated thickenings in secondary xylem. *Protoplasma* **233,** 255–262.

Rasband W.S. (1997–2011) *ImageJ*. National Institutes of Health, Bethesda, MD, USA. URL http://rsbweb.nih.gov/ij/.

Roberts A.G. (2005) Plasmodesmal structure and development. In *Plasmodesmata* (ed. K.J. Oparka), pp. 1–23. Blackwell, Oxford, UK.

Roth-Nebelsick A., Voigt D. & Gorb S. (2010) Cryo-scanning electron microscopy studies of *Pinus wallichiana* and *Mallotus japonicus*. *International Association of Wood Anatomists Journal* **31,** 257–267.

Russow E. (1883) Zur Kenntniss des Holzes, insonderheit des Coniferenholzes. *Botanisches Zentralblatt* **13,** 134–144.

Sanio K. (1873) Anatomie der gemeinen Kiefer (*Pinus silvestris* L.). *Jahrbücher für wissenschaftliche Botanik* **9,** 50–126.

Sano Y., Kawakami Y. & Ohtani J. (1999) Variation in the structure of intertracheary pit membranes in *Abies sachalinensis*, as observed by field-emission scanning electron microscopy. *International Association of Wood Anatomists Journal* **20,** 375–388.

Schacht H. (1859) Über die Tüpfel der Gefäss-und Holzzellen. *Botanische Zeitung* **17,** 238–239.

Schoonmaker A.L., Hacke U.G., Landhausser S.M., Lieffers V.J. & Tyree M.T. (2010) Hydraulic acclimation to shading in boreal conifers of varying shade tolerance. *Plant, Cell & Environment* **33,** 382–393.

Singh A., Dawson B., Franich R., Cowan F. & Warnes J. (1999) The relationship between pit membrane ultrastructure and chemical impregnability of wood. *Holzforschung* **53,** 341–346.

Sperry J.S. & Tyree M.T. (1988) Mechanism of water stress-induced xylem embolism. *Plant Physiology* **88,** 581–587.

Sperry J.S. & Tyree M.T. (1990) Water-stress-induced xylem embolism in three species of conifers. *Plant, Cell & Environment* **13,** 427–436.

Sperry J.S., Saliendra N.Z., Pockman W.T., Cochard H., Cruiziat P., Davis S.D., Ewers F.W. & Tyree M.T. (1996) New evidence for large negative xylem pressure and their measurements by the pressure chamber method. *Plant, Cell & Environment* **19,** 427–436.

Strasburger E. (1891) *Über den bau und die Verrichtungen der Leitungsbahnen in den Pflanzen*. Gustav Fischer, Jena, Germany.

Thomas R.J. (1969) The ultrastructure of southern pine bordered pit membranes as revealed by specialized drying techniques. *Wood and Fiber* **1,** 110–123.

Thomas R.J. & Nicholas D.D. (1969) The ultrastructure of the ray tracheid bordered pit membranes in southern pine. *Technical*

Association of the Pulp and Paper Industry Journal **52,** 2160–2163.

Tyree M.T. & Zimmermann M.H. (2002) *Xylem Structure and the Ascent of Sap*. Springer-Verlag, Berlin, Germany.

Usta I. & Hale M.D. (2006) Comparison of the bordered pits of two species of spruce (Pinaceae) in a green and kiln-dried condition and their effects on fluid flow in the stem wood in relation to wood preservation. *Forestry* **79,** 467–475.

Von Nägeli C. (1864) Aufquellende Epidermiszellen von Samen und Früchten. Sitzungsberichte der königliche bayerische Akademie der Wissenschaften Jahrgang 1864 Band II, 114–170.

Received 20 June 2011; accepted for publication 9 December 2011

SUPPORTING INFORMATION

Additional Supporting Information may be found in the online version of this article:

Figure S1. Box plot illustrating a significant difference ($P < 0.0001$) in S_{50} between species with punctured tori ($n = 13$) and non-punctured tori ($n = 20$). This difference remained significant ($P = 0.024$) when controlling for taxonomy based on a mixed model (see Material and methods for details).

Figure S2. Scaling of pit aperture diameter (D_a) versus pit membrane diameter (D_m, grey dots), and D_a versus torus diameter (D_t, black dots) as based on average values (±SD) for 13 species with punctured tori. All linear regressions were highly significant. These relationships remain significant ($P < 0.0001$) when controlling for taxonomy.

Table S1. List of pit morphological dimensions for 13 conifer species with punctured tori. Average and maximum pore sizes per species were based on SEM ($n \geq 25$) and TEM ($n \geq 5$) measurements. D_m, D_t and D_a were measured on a minimum of 15 aspirated pit membranes in order to obtain these parameters from the same pit. The TEM characters T_t and D_p were averaged for a minimum of 10 measurements. Av = average; Max = maximum; D_m = pit membrane diameter; D_t = torus diameter; D_a = aperture diameter; T_t = torus thickness; D_p = depth of the pit chamber; / = no pores were detected with TEM; X = species not studied with TEM.